Pulse compression using a tapered microstructure optical fiber

Jonathan Hu, Brian S. Marks, and Curtis R. Menyuk

University of Maryland Baltimore County, TRC 205A
5200 Westland Blvd., Baltimore, MD 21227

hu1@umbc.edu
http://www.photonics.umbc.edu/

Jinchae Kim

Department of Information and Communications,
Gwangju Institute of Science and Technology
1 Oryong-dong, Buk-gu, Gwangju, 500-712 Korea

Thomas F. Carruthers, Barbara M. Wright,
Thierry F. Taunay, and E. Joseph Friebele

Naval Research Laboratory, Washington, DC 20375

Abstract: We calculate the pulse compression in a tapered microstructure optical fiber with four layers of holes. We show that the primary limitation on pulse compression is the loss due to mode leakage. As a fiber's diameter decreases due to the tapering, so does the air-hole diameter, and at a sufficiently small diameter the guided mode loss becomes unacceptably high. For the four-layer geometry we considered, a compression factor of 10 can be achieved by a pulse with an initial FWHM duration of 3 ps in a tapered fiber that is 28 m long. We find that there is little difference in the pulse compression between a linear taper profile and a Gaussian taper profile. More layers of air-holes allows the pitch to decrease considerably before losses become unacceptable, but only a moderate increase in the degree of pulse compression is obtained.

OCIS codes: (000.4430) Numerical approximation and analysis; (060.4370) Nonlinear optics, fibers; (230.3990) Microstructure devices;

References and links

1. S. V. Chernikov and P. V. Mamyshev, "Femtosecond soliton propagation in fibers with slowly decreasing dispersion," J. Opt. Soc. Am. B **8**, 1633–1641 (1991).
2. N. A. Mortensen, "Effective area of photonic crystal fibers," Opt. Express **10**, 341–348 (2002), http://www.opticsexpress.org/abstract.cfm?URI=OPEX-10-7-341.
3. Y. Youk, D. Y. Kim, K. W. Park, "Guiding properties of a tapered photonic crystal fiber compared with those of a tapered single-mode fiber," Fiber Int. Opt. **23**, 439–446 (2004).
4. M. Foster, K. Moll, and A. Gaeta, "Optimal waveguide dimensions for nonlinear interactions," Opt. Express **12**, 2880–2887 (2004), http://www.opticsinfobase.org/abstract.cfm?URI=oe-12-13-2880.
5. T. P. White, B. T. Kuhlmey, R. C. McPhedran, D. Maystre, G. Renversez, C. M. de Sterke, and L. C. Botten, "Multipole method for microstructured optical fibers. I. Formulation," J. Opt. Soc. Am. B **19**, 2322–2330 (2002).
6. B. T. Kuhlmey, T. P. White, G. Renversez, D. Maystre, L. C. Botten, C. M. de Sterke, R. C. McPhedran, "Multipole method for microstructured optical fibers. II. Implementation and results," J. Opt. Soc. Am. B **19**, 2331–2340 (2002).

#68292 - $15.00 USD Received 3 March 2006; revised 12 April 2006; accepted 18 April 2006

7. B. T. Kuhlmey, R. C. McPhedran, C. M. de Sterke, P. A. Robinson, G. Renversez, and D. Maystre, "Microstructured optical fibers: where's the edge?," Opt. Express **10**, 1285–1290 (2002), http://www.opticsexpress.org/abstract.cfm?URI=OPEX-10-22-1285.
8. H. C. Nguyen, B. T. Kuhlmey, M. J. Steel, C. L. Smith, E. C. Mägi, R. C. McPhedran, and B. J. Eggleton, "Leakage of the fundamental mode in photonic crystal fiber tapers," Opt. Lett. **30**, 1123–1125 (2005).
9. X. Liu, C. Xu, W. H. Knox, J. K. Chandalia, B. J. Eggleton, S. G. Kosinski, and R. S. Windeler "Soliton self-frequency shift in a short tapered air-silica microstructure fiber," Opt. Lett. **26**, 358–360 (2001).
10. J. K. Chandalia, B. J. Eggleton, R. S. Windeler, S. G. Kosinski, X. Liu and C. Xu "Adiabatic coupling in tapered air-silica microstructured optical fiber," IEEE Photonics Technol. Lett. **13**, 52–54 (2001).
11. S. G. Leon-Saval, T. A. Birks, W. J. Wadsworth, P. St. J. Russell, and M. W. Mason, "Supercontinuum generation in submicron fibre waveguides," Opt. Express **12**, 2864–2869 (2004), http://www.opticsexpress.org/abstract.cfm?URI=OPEX-12-13-2864.
12. D. J. Moss, Y. Miao, V. Ta'eed, E. C. Mägi, and B. J. Eggleton, "Coupling to high-index waveguides via tapered microstructured optical fibre," Electron. Lett. **41**, 951–953 (2005).
13. G. E. Town and J. T. Lizier, "Tapered holey fibers for spot-size and numerical-aperture conversion," Opt. Lett. **26**, 1042–1044 (2001).
14. M. A. Foster and A. L. Gaeta, "Ultra-low threshold supercontinuum generation in sub-wavelength waveguides," Opt. Express **12**, 3137–3143 (2004), http://www.opticsexpress.org/abstract.cfm?URI=OPEX-12-14-3137.
15. M. Foster, A. Gaeta, Q. Cao, and R. Trebino, "Soliton-effect compression of supercontinuum to few-cycle durations in photonic nanowires," Opt. Express **13**, 6848–6855 (2005), http://www.opticsinfobase.org/abstract.cfm?URI=oe-13-18-6848.
16. Y. K. Lizé, E. C. Mägi, V. G. Ta'eed, J. A. Bolger, P. Steinvurzel, and B. J. Eggleton, "Microstructured optical fiber photonic wires with subwavelength core diameter," Opt. Express **12**, 3209–3217 (2004), http://www.opticsexpress.org/abstract.cfm?URI=OPEX-12-14-3209.
17. E. C. Mägi, P. Steinvurzel, and B. J. Eggleton, "Transverse characterization of tapered photonic crystal fibers," J. Appl. Phys. **96**, 3976–3982 (2004).
18. S. V. Chernikov, E. M. Dianov, D. J. Richardson, and D. N. Payne, "Soliton pulse compression in dispersion-decreasing fiber," Opt. Lett. **18**, 476–478 (1993).
19. H. H. Kuehl, "Solitons on an axially nonuniform optical fiber," J. Opt. Soc. Am. B **5**, 709–713 (1988).
20. J. Lægsgaard, N. A. Mortensen, and A. Bjarklev, "Mode areas and field-energy distribution in honeycomb photonic bandgap fibers," J. Opt. Soc. Am. B **20**, 2037–2045 (2003).
21. G. P. Agrawal, *Nonlinear Fiber Optics*, (3rd ed., Academic Press, San Diego, CA, 2001).
22. A. M. Zheltikov, "The physical limit for the waveguide enhancement of nonlinear-optical processes," Optics and Spectroscopy **95**, 410–415 (2003).
23. D. Marcuse, "Solution of the vector wave equation for general dielectric waveguides by the Galerkin method," IEEE J. Quantum Electron. **28**, 459–465 (1992).
24. J. Kim, U.-C. Paek, D. Y. Kim, and Y. Chung, "Analysis of the dispersion properties of holey optical fibers using normalized dispersion," in *Optical Fiber Communication Conference*, OSA Technical Digest (Optical Society of America, Washington DC, 2001), WDD86-1.
25. O. V. Sinkin, R. Holzlöhner, J. Zweck, and C. R. Menyuk, "Optimization of the Split-Step Fourier Method in Modeling Optical-Fiber Communications Systems," J. Lightwave Technol. **21**, 61–68 (2003).
26. K. J. Blow, N. J. Doran, and D. Wood, "Generation and stabilization of short soliton pulses in the amplified nonlinear Schrodinger equation," J. Opt. Soc. Am. B **5**, 381–391 (1988).
27. H. Kubota, K. Suzuki, S. Kawanishi, M. Nakazawa, M. Tanaka, and M. Fujita, "Low-loss, 2 km-long photonics crystal fiber with zero GVD in the near IR suitable for picosecond pulse propagation at the 800 nm band," Conference on Lasers and Electro-Optics, Baltimore, MD, 2001, paper CPD3-1.
28. M. D. Pelusi and H.-F. Liu, "Higher order soliton pulse compression in dispersion-decreasing optical fibers," IEEE J. Quantum Electron. **33**, 1430–1439 (1997).
29. A. Mostofi, H. Hatami-Hanza, and P. L. Chu, "Optimum dispersion profile for compression of fundamental solitons in dispersion decreasing fibers," IEEE J. Quantum Electron. **33**, 620–628 (1997).
30. M. D. Pelusi, Y. Matsui, and A. Suzuki, "Design of short dispersion decreasing fibre for enhanced compression of higher-order soliton pulses around 1550 nm," Electron. Lett. **35**, 61–63 (1999).
31. T. A. Birks and Y. W. Li, "The shape of fiber tapers," J. Lightwave Technol. **10,** 432–438, (1992).
32. W. H. Press, S. A. Teukolsky, W. T. Vetterling, and B. P. Flannery, in *Numerical Recipes in C++*, (2nd ed., Cambridge University Press, Cambridge, UK, 2003), Chap. 10.2, pp. 406–410.
33. E. H. Khoo, A. Q. Liu, and J. H. Wu, "Nonuniform photonic crystal taper for high-efficiency mode coupling," Opt. Express **13**, 7748-7759 (2005), http://www.opticsexpress.org/abstract.cfm?URI=OPEX-13-20-7748.

#68292 - $15.00 USD Received 3 March 2006; revised 12 April 2006; accepted 18 April 2006

1. Introduction

In previous work on dispersion-decreasing fibers, it was found that the dispersion decreases while the effective mode diameter remains almost constant [1]. By contrast, when one tapers microstructure optical fiber (MOF), the effective area and confinement loss also change [2, 3, 4]. Using the multipole method [5, 6], we find the lowest-order mode of a tapered fiber, as well as its corresponding dispersion, effective area and confinement loss. We determine the dependence of these parameters on the pitch — the distance between the centers of the holes. We find that the maximum transverse mode compression is limited by the confinement loss in the microstructure fiber, when the mode leaks beyond the last ring of holes. This result is consistent with recently reported work by Kuhlmey, *et al.* [7] and by Nguyen, *et al.* [8]. In the work reported here, we focus on a detailed study of the fundamental mode evolution in a four-ring structure that is appropriate for achieving nonlinear pulse compression.

To date, tapered MOF has been used to generate a soliton self-frequency shift [9, 10], to make a submicron waveguide [11], to couple waveguides [12], to convert numerical-aperture [13], to generate a supercontinuum [14, 15] and to make photonic wires [16]. However, the use of tapered MOF for pulse compression has not been reported in the literature. In this paper, we calculate the pulse compression that is achievable when we use realistic parameters for the dispersion, nonlinearity, and loss as the fiber is tapered, assuming that the transverse structure is preserved while tapering [8, 17]. We proceed by first determining the minimum size to which we can taper the fiber before loss becomes significant [7]. We then determine the compression factor of an input pulse by calculating its evolution in the tapered MOF using the nonlinear Schrödinger equation. The fiber diameter that we considered in this paper decreases monotonically.

As has been demonstrated in previous work on tapered or dispersion-decreasing fiber, the pulse evolution in these fibers depends on the pulse power, pulse duration, and the fiber properties, including the taper length [1, 18, 19]. We show theoretically in this paper that we can achieve a compression factor of 10 in a 28-m long tapered MOF, with an input pulse whose average input power and full-width half-maximum (FWHM) are 400 mw and 3 ps, respectively. The corresponding peak power is 11.8 W in a 10 Gb/s system. The compression factor is defined as the ratio of the FWHM pulse duration at the beginning and the end of the taper. By varying parameters, we have found that increasing the input power leads to larger compression factors and hence shorter pulses. By contrast, increasing the input pulse duration increases the compression factor but also increases the output pulse duration.

2. MOF Analysis

We used the multipole method to solve for the dispersion, effective area, and loss of the lowest-order mode, given our specific geometry — a hexagonal pattern with four layers of air holes [5, 6]. Figures 1 and 2 show the dispersion and confinement loss of the MOF as a function of pitch. The red solid, green dashed-dot, and blue dashed curves are for air-filling factors of 0.5, 0.55, and 0.6, respectively. The air-filling factor (AFF) is defined as the ratio of the hole diameter to the pitch. The ratio of the core diameter to the pitch is $(2\Lambda - \mathrm{AFF}\cdot\Lambda)/\Lambda = 2 - \mathrm{AFF}$. The wavelength used in the simulation is 1.55 μm. Figure 2 shows that as the pitch decreases, the matrix of holes fails to confine the mode, and the loss increases sharply. The pitch at which the sharp increase in loss occurs decreases as the air-filling factor increases, which is expected since a MOF with a larger air-filling factor has better mode confinement. The advantage of smaller pitch is that the fiber has smaller dispersion, which is also shown in Fig. 1.

Another parameter that changes when one tapers MOF is the nonlinear coefficient. The nonlinear coefficient is given by $\gamma(z) = \bar{n}_2(z)\omega_0/cA_{\mathrm{eff}}(z)$. We define the average nonlinear coeffi-

#68292 - $15.00 USD Received 3 March 2006; revised 12 April 2006; accepted 18 April 2006

cient $\bar{n}_2(x,y)$ and effective area A_{eff} as

$$\bar{n}_2 = \frac{\int\int_{-\infty}^{\infty} n_2(x,y)|S_z(x,y)|^2 dxdy}{\int\int_{-\infty}^{\infty} |S_z(x,y)|^2 dxdy},\ A_{\text{eff}} = \frac{(\int\int_{-\infty}^{\infty} |S_z(x,y)|dxdy)^2}{\int\int_{-\infty}^{\infty} |S_z(x,y)|^2 dxdy}, \tag{1}$$

where $n_2(x,y) = 2.6 \times 10^{-16}$ cm^2/W if the point (x,y) is located in the fused silica glass and $n_2(x,y) = 0$ if (x,y) is located in a hole. This definition takes into account the reduction in the nonlinear coefficient because the air holes do not contribute [20]. The quantity $|S_z|$ represents the magnitude of the longitudinal component of the Poynting vector. The effective area calculated using the z-component of the Poynting vector is the same for practical purposes as the effective area calculated using the squared magnitude of the electric field [21]. The variables ω_0 and c are the channel's central angular frequency and the speed of light, respectively. The variation of γ as a function of z comes from the variation in both $\bar{n}_2$ and A_{eff} with the pitch. Figure 3 shows that the effective area reaches its minimum when the pitch is about 1.5 μm [22]. We also found that $\bar{n}_2$ only changes by 4% over the range of pitch that we considered. We validated our code by comparing the dispersion and effective area with the result from the Galerkin method [23, 24]. These results are shown as crosses in Figs. 1 and 3 for the air-filling factor of 0.6. The loss cannot be obtained by the Galerkin method since this method assumes an infinite periodic structure. We note that the results presented here from both the multipole code and the Galerkin code used codes that we wrote ourselves. We obtain excellent agreement between the multipole method and Galerkin method for the group velocity dispersion and effective area.

The animation in Fig. 4 shows the four-layer MOF geometry that we used in our simulations and the corresponding mode profile. The air-filling factor used for the mode profile in this plot is 0.6. The black circles represent the hole boundaries and the contour plot represents the magnitude of the Poynting vector $|S_z|$. In the contour plot, we normalized $|S_z| = 1$ at the center, and plot the contours on a log scale from 10^{-1} to 10^{-6}. The left plot shows the geometry of the fiber and mode drawn to scale, while the right plot shows the geometry on a fixed scale normalized to the initial pitch value. When the pitch is large, the mode is well confined, but when the pitch decreases, the effective area becomes smaller. However, the mode diameter decreases more slowly than the pitch, and eventually the mode leaks past the outer air hole ring. We observe that the mode has spread to the outer air hole ring when the pitch is small. A sharp increase of the loss is then visible.

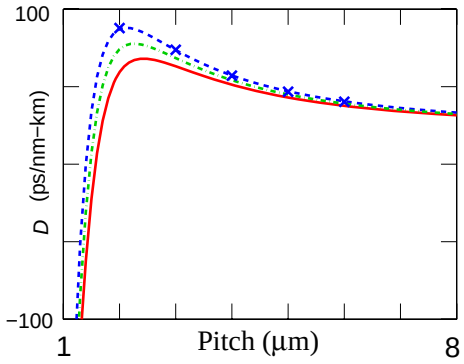

Fig. 1. The MOF mode dispersion as a function of pitch. The red solid, green dashed-dot, and blue dashed curves correspond, respectively, to air-filling factors of 0.5, 0.55, and 0.6 and are calculated using the multipole method. The crosses indicate results from the Galerkin method with an air-filling factor of 0.6.

#68292 - $15.00 USD Received 3 March 2006; revised 12 April 2006; accepted 18 April 2006

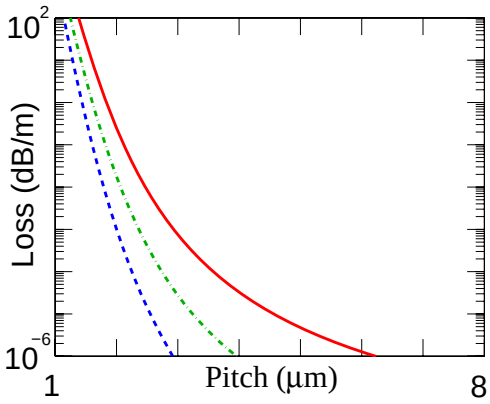

Fig. 2. The MOF mode loss as a function of pitch, calculated using the multipole method. The red solid, green dashed-dot, and blue dashed curves correspond, respectively, to air-filling factors of 0.5, 0.55, and 0.6.

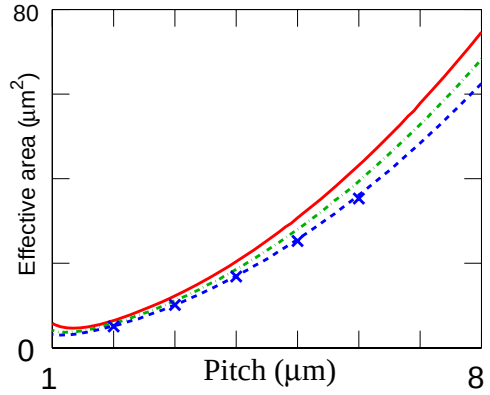

Fig. 3. The MOF effective area as a function of pitch. The red solid, green dashed-dot, and blue dashed curves correspond, respectively, to air-filling factors of 0.5, 0.55, and 0.6 and are calculated using the multipole method. The crosses indicate results from the Galerkin method with an air-filling factor of 0.6.

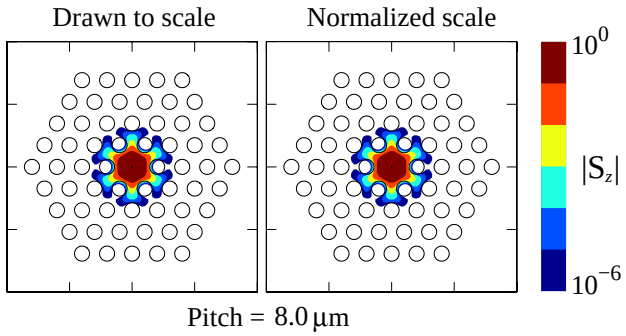

Fig. 4. (912 KB) Animation of the four-layer MOF geometry and mode profile. The black circles show the holes. The color contour plot represents the magnitude of the Poynting vector $|S_z|$. The air-filling factor is 0.6.

#68292 - $15.00 USD
Received 3 March 2006; revised 12 April 2006; accepted 18 April 2006

3. Pulse Propagation

The propagation of pulses in an optical fiber with variable dispersion and effective area can be described by the nonlinear Schrödinger equation (NLS) [21, 25, 26]

$$i\frac{\partial u}{\partial z} - \frac{1}{2}\beta_2(z)\frac{\partial^2 u}{\partial t^2} + \gamma(z)|u|^2 u + i\frac{\alpha}{2}u = 0, \tag{2}$$

where u is the complex electric field envelope, z is the distance along the fiber, and t is retarded time. The fiber is taken to be nonuniform, so that the dispersion $\beta_2(z) = -\lambda^2 D(z)/2\pi c$ depends on z. The nonlinear coefficient $\gamma(z)$ was defined in the Sec. 2. The parameter α represents the fiber's intrinsic loss, which we fix at 0.02 dB/m, see for example [27]. We solve the nonlinear Schrödinger equation using a standard split-step Fourier method for various initial pulse durations and powers to explore the effect of the taper on the pulse compression [21, 25].

Soliton compression can be used to compress pulses [28], but this compression normally yields a large pedestal. In principle, one can achieve nearly pedestal-free compression with a lower input power by adiabatic pulse compression [29, 30]. However, the fiber must be far longer than the nonlinear scale length all along the taper, leading to a tradeoff. A faster taper uses the fiber more efficiently but produces a larger pedestal.

When solving the NLS equation with dispersion-decreasing fibers, one need only consider changes to the dispersion along the fiber [28, 29]. By contrast, when solving the NLS equation with tapered MOF, one must consider both changes in the dispersion and effective area. We have observed that it is possible to compress the pulse while the dispersion increases by propagating it through tapered MOF, due to the simultaneous decrease in the effective area.

4. Results and Analysis

In our simulations, we considered both linear and Gaussian taper profiles for the pitch as a function of distance [29, 31]. The pitch was reduced from 4.5 μm to 1.8 μm. We choose a lower limit of 1.8 μm so that the loss threshold was not crossed. The calculated confinement loss for a four-layer MOF with pitches of 1.7 and 1.8 μm are 0.03 dB/m and 0.0088 dB/m, respectively. The calculated dispersion with a 1.8 μm pitch is 79.4 ps/nm-km. We used a starting pitch of 4.5 μm, which is the maximum possible value due to the constraints of fiber drawing. The linear profile is determined by the fiber pitch at the beginning and the end, so that $P(z) = [(L-z)P(0) + zP(L)]/L$, where P is the pitch. The Gaussian taper profile is described by the formula $P(z) = P(0)\exp(-z^2/\sigma^2)$, where σ is chosen so that $P(L)$ = 1.8 μm. We solved the nonlinear Schrödinger equation to propagate short pulses along the tapered MOF taking into account second-order dispersion, nonlinearity, and loss. In order to obtain the best compression, we used Brent's method to determine the optimal fiber length [32]. Losses due to reflection have been ignored, since the taper length is much longer than a wavelength. This assumption is consistent with what has been observed in simulations of photonic crystal tapers [33]. In Fig. 5, we show contour plots for the optimized compression factor for a hyperbolic-secant-shaped pulse when the fiber length is varied. Figures 5(a) and (b) correspond to linear and Gaussian taper profiles, respectively. In these contour plots, the *x*-axis represents the input pulse FWHM, which ranges from 1 ps to 4 ps. The *y*-axis shows the average input power, which varies from 300 mW to 700 mW. The repetition rate is 10 Gb/s. The 300 mW to 700 mW average power with a 3-ps input pulse FWHM correspond to 8.8 W and 20.6 W peak power. The wavelength used here is 1.55 μm. In Fig. 6, we show contour plots for the final pulse duration with (a) linear and (b) Gaussian taper profiles. Figures 5 and 6 show that increasing the input power leads to larger compression and hence shorter pulses. By contrast, increasing the input pulse duration increases the compression factor but also increases the output pulse duration. There is little difference between the contour plots in Figs. 5 and 6.

#68292 - $15.00 USD Received 3 March 2006; revised 12 April 2006; accepted 18 April 2006

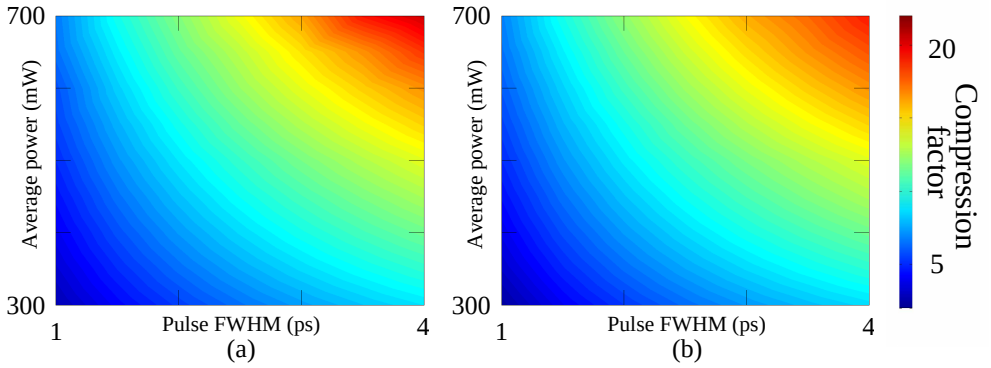

Fig. 5. The contour plot for the optimized compression factor for a hyperbolic-secant-shaped pulse when the fiber length is varied using (a) a linear and (b) a Gaussian taper profile. In this contour plot, the *x*-axis represents input pulse FWHM, which varies from 1 ps to 4 ps. The *y*-axis presents the average input power, which varies from 300 mW to 700 mW. We use a 10 Gb/s repetition rate in our simulation.

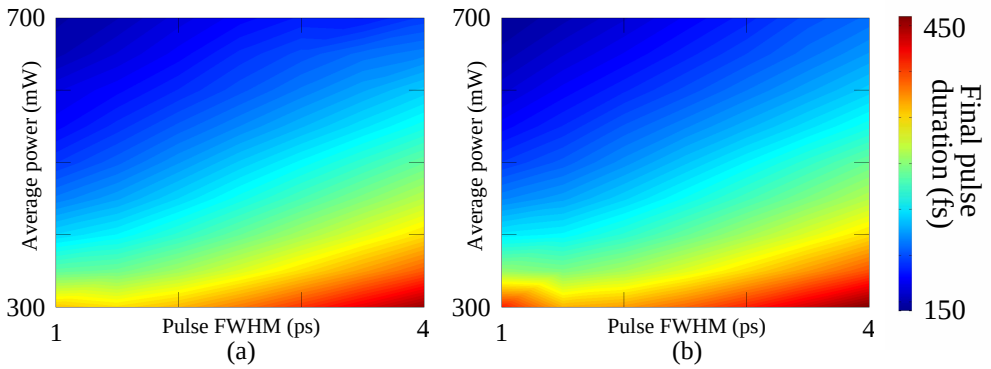

Fig. 6. The contour plot for the output pulse FWHM factor for a hyperbolic-secant-shaped pulse when the fiber length is varied using (a) a linear and (b) a Gaussian taper profile. In this contour plot, the *x*-axis represents input pulse FWHM, which varies from 1 ps to 4 ps. The *y*-axis presents an input average power that varies from 300 mW to 700 mW. We use a 10 Gb/s repetition rate in our simulation.

#68292 - $15.00 USD
Received 3 March 2006; revised 12 April 2006; accepted 18 April 2006

In order to test the sensitivity of the tapered draw to changes in the fiber length, we also plot the compression factor, in Figs. 7 as a function of fiber length for an input pulse FWHM of (a) 1 ps, (b) 2 ps, (c) 3 ps, and (d) 4 ps with 500 mW average input power, (e) 3 ps with 400 mW average input power, and (f) 3 ps with 300 mW average input power. The red solid and blue dashed curves represent linear and Gaussian taper profiles, respectively. As one can observe, the compression factor oscillates with the fiber length. Energy transfers from the central portion of the pulse to its pedestal as a function of distance causes this oscillation. These data show that the fiber length should be carefully chosen to obtain optimal pulse compression. Additionally, we find that the compression factor curves oscillate less at lower power values as shown in Figs. 7(e) and (f). With 500 mW average input power, the optimized lengths are 8.9 m, 14.7 m, 39.9 m, and 55.5 m corresponding to 1-ps, 2-ps, 3-ps, and 4-ps input FWHM pulses with a linear taper profile. We also show the compression factor as a function of fiber length for an input pulse FWHM of (a) 1 ps, (b) 2 ps, (c) 3 ps, and (d) 4 ps with a peak input power of 10 W in Figs. 8. The corresponding average powers are 114 mW, 227 mW, 340 mW, and 454 mW. We note that in Fig. 8(a), there is no pulse compression since the nonlinearity is too low. The average power of 114 mW in this case is lower than the average power shown in Figs. 5 and 6. With a peak input power of 10 W, the optimized lengths are 46.9 m, 33.7 m, and 34.0 m corresponding to 2-ps, 3-ps, and 4-ps input FWHM pulses with a linear taper profile.

Figure 9 shows the optimized pitch evolution for a 3-ps input pulse with an average power of 400 mW or peak power of 11.8 W with linear (red) and Gaussian (blue) taper profiles. The compression factor is optimized by choosing the length to correspond to the highest peak in Fig. 7(e). In Fig. 10, the green curve represents the 3-ps input pulse. The red solid and blue dashed curves represent the output pulses after transmission through the MOF with the linear and Gaussian taper profiles, respectively, shown in Fig. 9. We find that there is little difference between the output pulse shapes when the linear or the Gaussian taper profile is used. Both of the output pulses have small pedestals whose amplitude is 2% of the maximum amplitude and contain 23% of the pulse energy.

In Fig. 7(e), we obtain a compression factor of 10 using a 28-m tapered MOF with four layers of air hole rings. We also ran our mode solver for the MOF with six layers of holes. We did find that the loss is smaller than 0.02 dB/m for all pitch values larger than 1.3 μm for the six-layer fiber. However, the dispersion and effective area only change by 0.1% as compared to the four-layer MOF within the pitch range of 4.5 μm and 1.5 μm. The calculated dispersions at 1.4 and 1.5 μm pitch are -0.4 and 34 ps/nm-km, respectively. Then we simulated a six-layer MOF to see how large the compression factor becomes when the final pitch is 1.5 μm, so that we obtain smaller dispersion. We found that the maximum compression factor for a 3-ps input pulse with an average power of 400 mW increases about 20% as compared to a four-layer MOF. In the case of a five-layer MOF, the calculated loss is smaller than 0.02 dB/m with all pitch values larger than 1.5 μm. We also obtained a similar result with 1-ps, 2-ps, and 4-ps input pulses. Additionally, we have tested the wavelength dependence of our fiber design. We find that the difference in the compression factor is smaller then 1.5%, when we compare wavelengths 1540 nm and 1560 nm. Lastly, we changed the starting pitch to 8 μm, keeping the final pitch at 1.5 μm. For this pitch range, we found a maximum compression factor of 12.6, as compared to the compression factor of 10 with a starting pitch of 4.5 μm.

#68292 - $15.00 USD Received 3 March 2006; revised 12 April 2006; accepted 18 April 2006

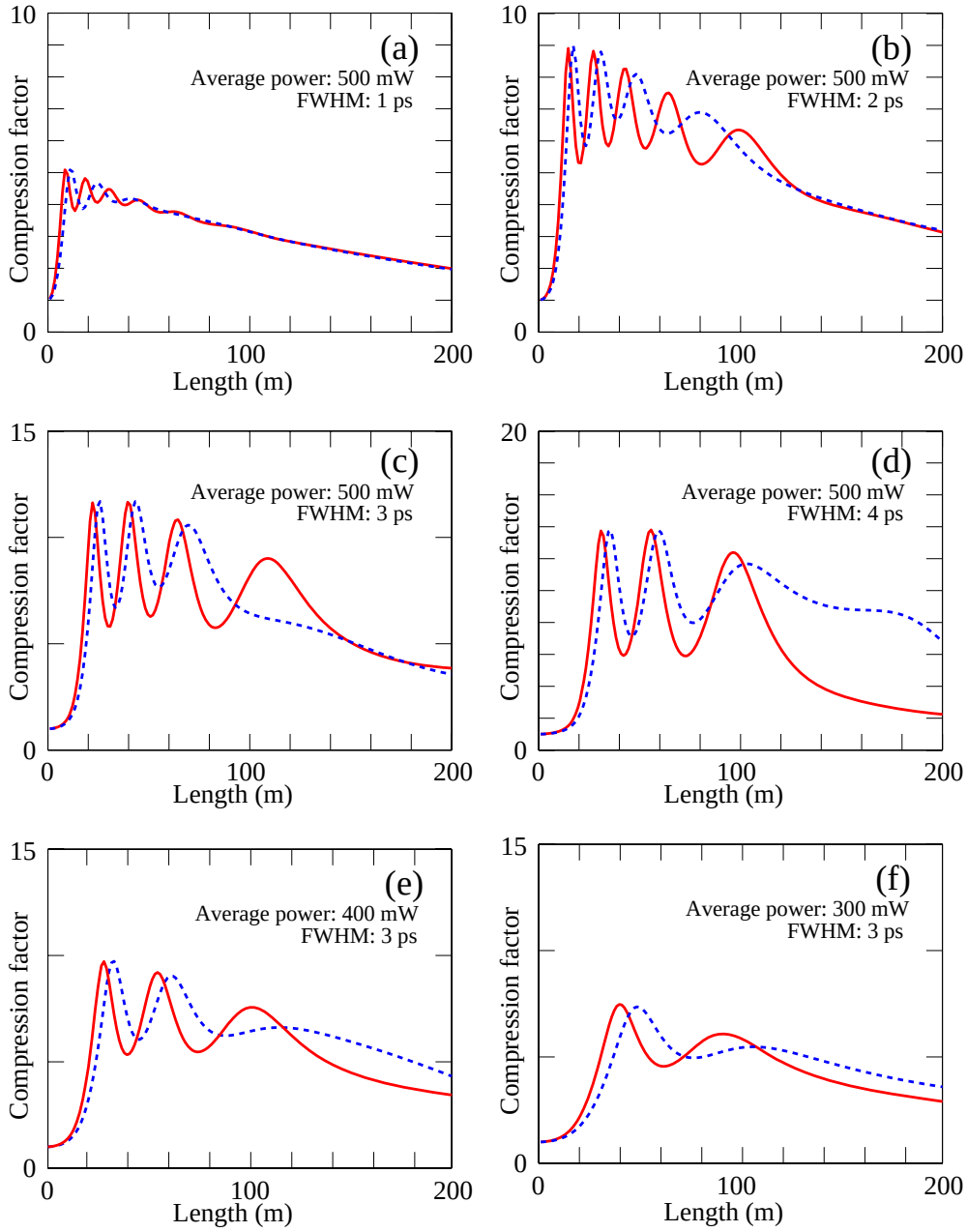

Fig. 7. Compression factor as a function of fiber length for an input pulse FWHM of (a) 1 ps, (b) 2 ps, (c) 3 ps, and (d) 4 ps with 500 mW average input power, (e) 3 ps with 400 mW average input power, and (f) 3 ps with 300 mW average input power. The corresponding peak powers are 44 W, 22 W, 14.7 W, 11 W, 11.8 W, and 8.8 W for (a), (b), (c), (d), (e), and (f), respectively. The red solid and blue dashed curves represent the linear and Gaussian taper profile, respectively.

#68292 - $15.00 USD
Received 3 March 2006; revised 12 April 2006; accepted 18 April 2006

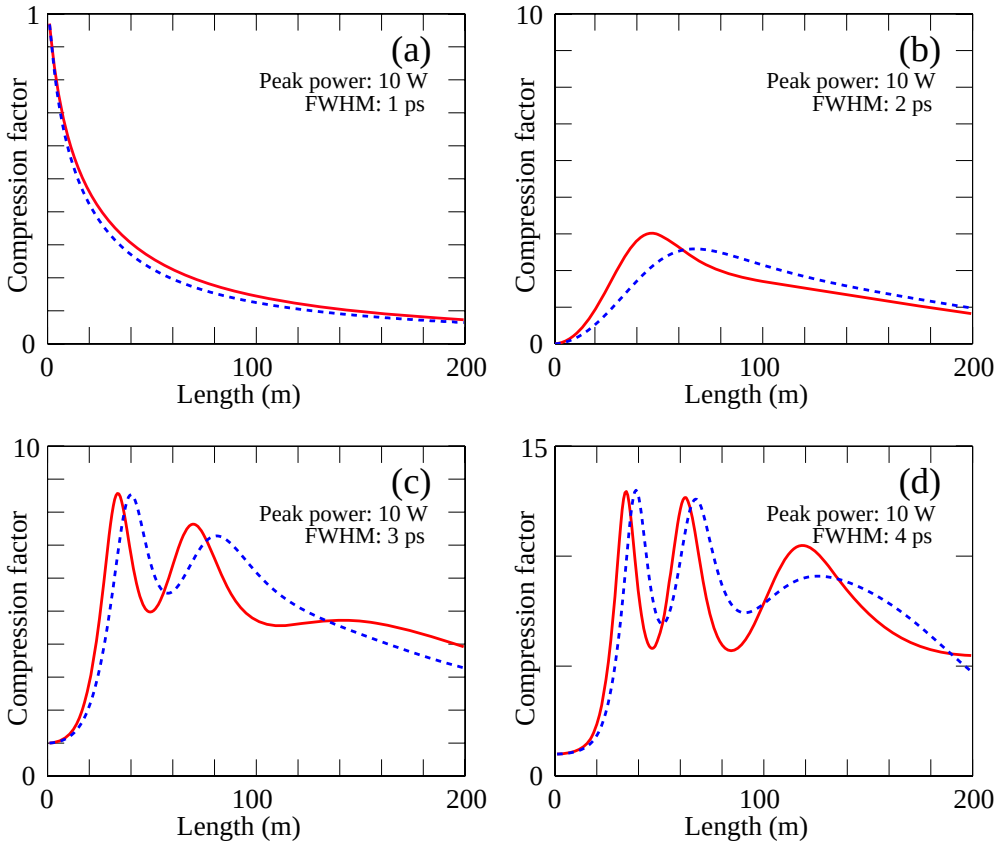

Fig. 8. Compression factor as a function of fiber length for an input pulse FWHM of (a) 1 ps, (b) 2 ps, (c) 3 ps, and (d) 4 ps with a peak input power of 10 W. The red solid and blue dashed curves represent the linear and Gaussian taper profile, respectively.

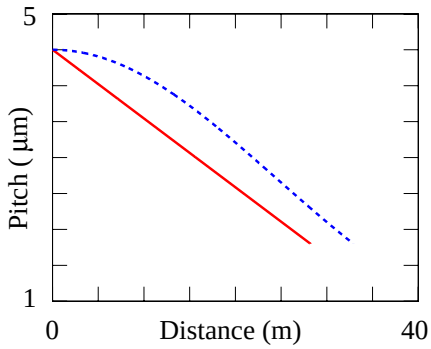

Fig. 9. Pitch as a function of distance. The red solid and blue dashed curves represent a linear and Gaussian taper profile, respectively.

#68292 - $15.00 USD
Received 3 March 2006; revised 12 April 2006; accepted 18 April 2006

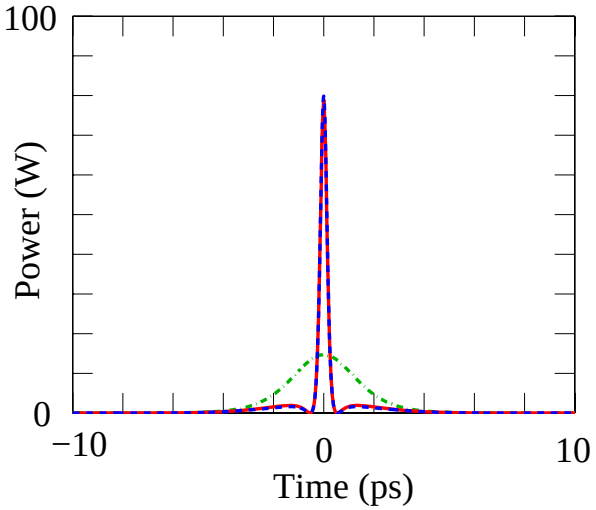

Fig. 10. Input and output pulse shapes for the tapered MOF. The green dash-dot curve represents the 3-ps input pulse. The red solid and blue dashed curves represent, respectively, the output pulses after transmission through the MOF with the linear and Gaussian taper profiles shown in Fig. 9.

5. Conclusion

Our simulations have combined a multipole mode solver with a nonlinear Schrödinger equation solver to study the achievable pulse compression in a tapered microstructure fiber. We have shown that the primary limitation to pulse compression in a four-layer tapered microstructure fiber is the loss due to mode leakage. We also found that the difference in the compression factor between a linear and Gaussian taper profile was negligible. For the four-layer geometry that we considered, a compression factor of 10 can be achieved by a pulse with an initial FWHM duration of 3 ps in a tapered fiber that is 28 m long.

Acknowledgments

We would like to thank B. Kuhlmey and Q. Zhang for many useful discussions.

#68292 - $15.00 USD Received 3 March 2006; revised 12 April 2006; accepted 18 April 2006